https://ntrs.nasa.gov/search.jsp?R=19650024112 2018-07-24T13:22:10+00:00Z

For Publication in the Physics of Fluids journal

[redacted]

[redacted]

Nasa CR-58153

RESEARCH NOTE 460

N65-33713

FACILITY FORM 602

(ACCESSION NUMBER)	(THRU)
36	1
(PAGES)	(CODE)
CR 58153	25
(NASA CR OR TMX OR AD NUMBER)	(CATEGORY)

EXPERIMENTS WITH MAGNETOHYDRODYNAMICALLY SUPPORTED SHOCK LAYERS

by

E. Locke, H. E. Petschek and P. H. Rose

AVCO-EVERETT RESEARCH LABORATORY
a division of
AVCO CORPORATION
Everett, Massachusetts

GPO PRICE $ _____

CSFTI PRICE(S) $ _____

Hard copy (HC) 2.00

Microfiche (MF) .50

ff 653 July 65

Contract No. NAS w-748

July 1964

prepared for

HEADQUARTERS
NATIONAL AERONAUTICS AND SPACE ADMINISTRATION
OFFICE OF ADVANCED RESEARCH AND TECHNOLOGY
Washington 25, D. C.

[redacted]

ABSTRACT

33713

Shock tube experiments have been performed to quantitatively determine the interaction of a hypersonic flow with the magnetic field of a straight current-carrying wire oriented perpendicular to the flow direction. The interaction which takes place in a thin layer behind a detached shock wave is subject to the following restrictions: (1) Negligible conductivity upstream of the shock; (2) Low magnetic Reynolds number and scalar conductivity in the shock layer. The straight wire geometry under these restrictions has been analyzed theoretically by Levy and Petschek. The analysis, which is briefly reviewed, predicts the location of a thin shock layer which is concentric with the wire.

Most of the experimental work was performed in a 50-50 mixture of argon and oxygen, at an initial pressure of 1 mm Hg, and in a range of shock velocities between 4.3 and 6 mm/μsec. Data have been obtained by observing the flow luminosity, using an image converter and mirror camera looking both perpendicular to and along the wire. A circular shock front was observed to stand up to 5-1/2 cm in front of a 1 cm radius cylinder producing the magnetic field. The data on shock position vs current were in excellent agreement with theory in spite of the fact that values of ϵ equal to 0.25 resulted in theoretical accuracies only to within a factor of two.

Author

[redacted]

SECTION I

INTRODUCTION

Since the earliest days of hypersonic atmospheric flight, speculations have been made about the useful application of magnetohydrodynamic principles to this regime. The obvious combination of the thermally ionized gases surrounding a vehicle in this environment, and strong magnetic fields, offers the attractive possibility of producing significant forces and other alterations of the natural flow about a vehicle without intimate contact between a solid surface and the hot gas, with the attendant reduction of heating. The first attempts at making this combination were thwarted by the realization that in general the energy transfer reduction to the vehicle was more than balanced by the joule dissipation in the field coils required to produce the MHD interaction. Recent advances in the area of superconducting field coils promise to alleviate this restriction and have created a new interest in flight applications of MHD.

Some of the MHD interactions of interest to this flight regime are in the low Magnetic Reynolds number region: a regime which has not received too much attention in the literature, particularly from the experimental point of view. The recent theoretical analysis of Levy and Petschek[1] of the two-dimensional hypersonic flow of a partially ionized gas over a straight current-carrying conductor provided a chance for a quantitative comparison of an experimental investigation of a flow of interest to the flight MHD problem with theory. The present paper reports the details of this experimental investigation.

A number of previous experiments have been reported which bear on this problem. The earliest experimental verification of a low Magnetic Reynolds number, MHD flow phenomena was the choking of a one-dimensional flow in an annular nozzle, supplied by a combustion driven shock tube, by Patrick and Brogan.[2] This experiment still remains as one of the few quantitative works in this field as they were able to predict the location of normal shocks in their nozzle from one-dimensional MHD channel flow considerations. Some time later Patrick[3] also produced the first MHD deflection of the flow about a body, a conical body in a shock tube operating in argon, by the magnetic field of a coil built into the surface of the cone. The strength of the conical bow shock was clearly increased by the magnetic field, but no quantitative results were obtained.

The possibility of producing lift with magnetic fields was the subject of a semi-quantitative two-dimensional experiment performed by Patrick.[4] For these experiments current was passed through a helix which had its axis perpendicular to the flow direction. The value of the magnetic field was made large enought to cause the Hall Parameter to be unity. This caused the gas

currents to have a component parallel to the flow direction, resulting in a lift force on the helix. The experimental data clearly showed a flow asymmetry, indicative of a lift force at conditions where a linear theory developed by Kemp and Petschek[5] had indicated that lift-drag ratios of order unity were possible.

The first attempt to produce a quantitative body MHD flow interaction was made by Ziemer.[6] With a coil built into the nose of a hemispherical model he attempted to reproduce the effect predicted by Bush.[7] Bush, as well as Kemp,[8] Neuringer[9] and Lykoudis[10] all predicted an effect on the stagnation point pressure and velocity gradient due to magnetic fields for small values of interaction parameter. Bush extended this analysis to larger values of interaction parameter and found that with increasing value of this parameter the shock stand-off distance also had to increase. This result was verified by Ziemer but the quantitative aspects of this work must be treated with suspicion. Ziemer used a magnetically-driven shock tube, similar to the type developed by Josephson.[11] In this type of device the existence of a homogeneous hot gas sample of known and calculable properties has not been established. In fact, considerable evidence exists that this end has not been achieved in these devices. Cloupeau[12] showed that the driver gases and test gas were indistinguishable. Keck[13] and Pugh[14] showed that the front in this type of device can be non-plane, curved, and even highly turbulent and that a clear separation of the driving mechanism from the test gas has not been achieved. In addition, Ziemer's conical shock tube has severe attenuation of shock velocity with distance and consequently in homogeneous gas conditions. Also, his data on test time are not consistent with continuity considerations. Thus, his quantitative analysis and comparison with the Bush theory must be regarded as suspect.

Two other related experiments should be mentioned. Ericson[15] attempted to produce an MHD interaction in a shock tunnel flow. After a number of runs which did not produce the expected interaction, one or several isolated experiments showed an unexpected effect. It was concluded that the ionization kinetics of the nozzle flow, as well as the bow shock, were not expected to be sufficiently fast in the nozzle to produce equilibrium or otherwise predictable conditions for this experiment.

The final investigation to be mentioned is the work of Bostick.[16] Bostick uses a plasma source to shoot a slug of plasma, a plasmoid, against a magnetic field produced by a wire normal to the plasma flow direction. In this experiment the plasma conductivity is essentially infinite but otherwise the plasma properties are not too well known. The results of this experiment generally agreed with the infinite conductivity calculations of Hurley.[17]

The present work is an attempt to reproduce the simple two-dimensional geometry analyzed by Levy and Petschek in an experiment which can be compared quantitatively with the theory. The interaction between the flow and the magnetic field, behind a shock wave standing ahead of the conductor, is investigated under the following restrictions:

1) The free stream is essentially non-conducting, characteristic of the flight situation.

2) The shock layer conductivity is low (low magnetic Reynolds number)

3) Scalar conductivity in the shock layer (Hall parameter small)

Emphasis was placed on the ability to achieve quantitative results; thus a facility in which the existence of a homogeneous gas sample with calculable gas properties was the prime requisite. The six-inch diameter arc-heated driver shock tube[18] fitted this requirement while producing the requisite gas properties in air. Later experiments with oxygen-argon mixtures could have been performed in combustion-driver shock tubes but for simplicity were also performed in the arc-driver facility. Sufficient measurements were taken and sufficient experience exists with this facility that the properties and thermodynamic state of the test gas was known with some confidence. Thus the observed flow interaction geometry could be connected to the theory in a quantitative manner. Probably the most serious uncertainty in this comparison is that the theory assumes a large density increase across the shock while in the experiments the density increase was only moderate.

In the next section, the theory of Levy and Petschek is reviewed briefly. Because the theory is a steady state description of the phenomenon and the experiment can be considered quasi-steady at best, the modifications of the theory required to apply it to the experimental situation are outlined in Section III. The experimental equipment and techniques used, followed by a presentation and discussion of the results, are presented in Sections IV and V. Section VI discusses the quantitative comparison with the Levy-Petschek theory and Section VII reiterates the major conclusions drawn from this experimental study.

SECTION II

REVIEW OF THEORY

A theoretical investigation of the MHD flow applicable to the present experiments has been performed by Levy and Petschek.[1] In this section, we will very briefly review the approach used, and the conclusions reached in that theory. The flow geometry analyzed is represented schematically in Fig. 1. The analysis was performed for the following conditions: (1) The free stream is nonconducting, (2) The magnetic field has a strong effect on the flow, i.e., a large interaction parameter, (3) The applied magnetic field is produced by an infinitely long current-carrying wire oriented perpendicular to the flow, and its field is not affected by the gas currents, (4) The gas conductivity is a scalar quantity.

In the analysis, the presence of a shock wave was assumed. An Analysis was then made to determine the location of this shock, and the flow field behind it. The change in magnetic field across the shock wave is small, so that the thermodynamic properties of the gas immediately behind the shock are described by the hydrodynamic shock equations. Hence, the interaction of the magnetic field with the flow in the vicinity of the stagnation streamline takes place in the region of subsonic flow behind a normal shock. This region, which a simple continuity analysis will show to be thin, is called the shock layer in Fig. 1. Momentum balance in this region requires that the magnetic force integrated across the layer be equal to the pressure behind the shock, or for hypersonic flow, the free stream dynamic pressure.

Thus roughly,

$$\left[\underset{\sim}{j}_s \times \underset{\sim}{B}(r_o)\right] = \rho_\infty U_\infty^{\,2} \tag{1}$$

The subscript s refers to conditions in the shock layer, and ∞ refers to the free stream conditions in front of the shock; $\underset{\sim}{j}_s$ is the current density, $\underset{\sim}{B}(r_o)$ is the magnetic field at the shock, which is located a distance r_o from the wire; δ the thickness of the layer, ρ_∞ and U_∞ the free stream density and velocity, respectively. The current density can be calculated from Ohm's law which, for small Hall parameters, may be written in terms of the gas conductivity σ_s as:

$$\underset{\sim}{j}_s = \sigma_s \left[\underset{\sim}{u}_s \times \underset{\sim}{B}(r_o)\right]$$

where $\underset{\sim}{u}_s$ is the velocity behind the normal shock, which is equal to $\epsilon \underset{\sim}{U}_\infty$ and ϵ is the ratio of the free stream density to the density in the shock layer. Hence, since $\underset{\sim}{B}$ is perpendicular to $\underset{\sim}{U}_\infty$, Eq. (1) becomes

$$\rho_\infty U_\infty^2 = \sigma_s \epsilon U_\infty B^2 (r_o) \delta \tag{2}$$

In order to determine the thickness of the shock layer, δ, it is necessary to take into account the curvature of the shock. Let ϕ be the inclination angle of $\underset{\sim}{r}_o$ measured from the stagnation streamline, and u and v be the radial and azimuthal components of velocity. From the oblique shock relation, we know

$$u_s = - \epsilon U_\infty \cos \phi$$

$$v_s = U_\infty \sin \phi$$

The mass flow entering a section of the shock layer which subtends an angle of ϕ along the shock, is $\rho_\infty U_\infty r_o \sin \phi$. This must equal the mass flow leaving in a radial direction: $\rho_s v_s \delta$. Equating these mass flow rates, and using the relation given above for v_s, we find that

$$\delta = \epsilon r_o \tag{3}$$

We now express the magnetic field B in terms of the distance r_o from the wire

$$B (r_o) = \frac{\mu_o I}{2 \pi r_o} \tag{4}$$

where μ_o is the permeability of free space, and I is the wire current. Substituting Eq. (4) and Eq. (3) into Eq. (2), and solving for r_o, we find

$$r_o = \frac{\sigma_s \epsilon^2}{\rho_\infty U_\infty} \left(\frac{\mu_o I}{2 \pi}\right)^2 \tag{5}$$

In this simple derivation, all quantities in the shock layer were described in terms of an average value, and it was assumed that (1) the center of curvature of the shock was at the wire, and (2) the forces in the azimuthal direction do not change the tangential velocity from its value just behind the shock. The more accurate analysis made by Petschek and Levy considered the flow in the stagnation region, including variations in flow properties in the shock layer and the effects of transverse pressure gradients. They

concluded that the shock follows magnetic field lines to the order of ϵ. The more accurate expressions for shock position and density profile from Ref. (1) are as follows:

$$\text{Shock position:} \quad r_o = \frac{\epsilon^2 \sigma_s}{\rho_\infty U_\infty} \left(\frac{\mu_o I}{2\pi}\right)^2 \left[\frac{3}{1 + \sqrt{2\epsilon}}\right] \tag{6}$$

$$\text{Density Profile:} \quad \frac{r_o - r}{\epsilon r_o} = \int_a^{a/\rho_s^*} \frac{dx}{\sqrt{1+x^3}} \tag{7}$$

where

$$a = \left[2\,(2\epsilon)^{1/2}\right]^{3/2} \left[1 + \sqrt{2\epsilon}\right] / 3$$

and

$$\rho_s^* = \rho_s \; \epsilon/\rho_\infty$$

These expressions were derived under the assumption of $\sqrt{2\epsilon} < 1$. As in the case of predicting the aerodynamic shock detachment distance, however, the analysis is expected to become less accurate for density ratios closer to unity.

SECTION III

APPLICATION OF THEORY TO SHOCK TUBE EXPERIMENT

The experimental study was carried out in a shock tube. The theoretical calculations must be modified to apply them to the conditions under which the experiment was performed, which includes the effects of a non-steady magnetic field. Calculations of the instantaneous shock position as a function of time are made based on a quasi-steady state theory.

The magnetic field for the experiments was produced by current generated by the discharge of a capacitor bank through a rod which was inserted across the diameter of the shock tube. The region of test gas between the incident shock, and the contact interface is the gas in which the experiment was performed. The properties of this "free stream" gas can be calculated from the normal shock relations for a moving shock, in terms of the shock speed, U_s and initial shock tube pressure, p_i.

As soon as the incident shock passes the wire, an aerodynamically supported shock must form around the wire. The region behind this shock is the region in which the interaction with the magnetic field first takes place. The gas conditions in this shock layer near the stagnation streamline are calculable by using the normal shock relation for a stationary shock. The conductivity σ_s in the shock layer is calculated from the relation:

$$\sigma_s = \frac{n_e e^2 \tau}{m_e}$$

Where $\tau_e = [\overline{C}_e \sum_j n_j \overline{Q}_j]^{-1}$ is the mean free time of the electron in the ionized mixture, n_e is the electron number density, e the charge on the electron, m_e the electron mass, $\overline{C}_e$ the mean thermal electron velocity, and n_j identifies the number density of the $j^{\underline{th}}$ species, which has a cross section for momentum transfer with electrons of magnitude Q_j. The values of the cross section for the gases used in our experiments have been taken from the literature.[19] The equilibrium values of temperature and species number densities are calculated from the Saha equation in the usual way. Calculations of the rate processes, as well as experimental data to be discussed later, indicate that the gas comes into thermodynamic equilibrium very quickly, justifying the use of the Saha equation.

The restriction that the free stream conductivity be small places an upper limit on the allowed incident shock velocity. The free stream conductivity will not be significant if the pressure exerted by the magnetic field across the shock layer is large compared to that exerted in the free stream.

Thus, small upstream conductivity implies that:

$$\int_{r_o}^{\infty} \underset{\sim}{j} \times \underset{\sim}{B} \cdot dr < \epsilon^2 \sigma_s U_\infty B_o^2 r_o$$

Expressing $\underset{\sim}{j}$ in the region between the shock position and infinity as

$\underset{\sim}{j} = \dfrac{\sigma_\infty U_\infty \underset{\sim}{B}(r)}{1+(\omega_e \tau_e)_\infty^2}$ we find that the limitation on upstream conductivity is

$$\frac{\sigma_s}{\sigma_\infty} > \frac{\pi/2}{\epsilon^2 (\omega_e \tau_e)_\infty} \left[1 - \frac{2}{\pi} \tan^{-1} \left(\frac{1}{\omega_e \tau_e} \right)_\infty \right]$$

where ω_e is the electron cyclotron frequency.

The restriction to small Hall coefficients places a lower limit on the allowed incident shock velocity. It was concluded by Levy and Petschek that the Hall parameter may be as large as $1/\epsilon$ due to the fact that a thin shock layer inhibits the flow of the Hall currents. Both of the shock velocity restrictions will be indicated quantitatively on future graphs.

Initially the flow geometry in the shock tube experiment is unsteady because the interaction parameters is larger than unity at the aerodynamically supported shock position. As a result, the shock layer will be pushed upstream until it reaches a position where Eq. (6) is satisfied. The time required for this to happen, i. e. the setup time for steady flow geometry should be shorter than both the test time and the characteristic quarter cycle time of the capacitor bank. An estimate of this time may be made by applying the momentum equation to the shock layer in a manner very similar to that explained in Section II, except that in the present case the shock layer is not considered to be stationary, but moving with a velocity dr_s/dt toward its steady state position r_o. Following the corresponding aerodynamic situation, it will be assumed that dr_s/dt is small compared with U_∞, and can be ignored compared with it. In the shock velocity range for which the experiments were performed, σ_s varied only as $T^{3/2}$. Hence, we may to a fair degree of accuracy, assume that σ_s is independent of dr_s/dt. Since the flow velocity behind the shock is ϵU_∞ relative to the shock, the current in the shock layer may be written as*

$$j_s = \sigma_s (\epsilon U_\infty + dr_s(t)/dt) B(r_s)$$

where $B(r_s) = \mu_o I/2\pi r_s$.

---

*The electric field associated with $\frac{\partial B}{\partial t}$ has been neglected in this equation since for the quarter cycle times used it is generally small.

Generalizing Eq. (3) to $\delta = \epsilon\, r_s$ and using the above expression for current Eq. (1) may be written as

$$\sigma_s \epsilon^2 U_\infty \left(\frac{\mu_o I}{2\pi}\right)^2 \frac{1}{r_s(t)} \left(1 - \frac{1}{\epsilon U_\infty} \frac{dr_s(t)}{dt}\right) = \rho_\infty U_\infty^2 \qquad (8)$$

This equation can be simplified by defining

$$r_o(t) = \frac{\sigma_s \epsilon^2}{\rho_\infty U_\infty} \left(\frac{\mu_o I(t)}{2\pi}\right)^2 \qquad (9)$$

which can be interpreted as the shock location which would correspond to a steady current whose magnitude was equal to the instantaneous current. Equation (8) now becomes

$$\frac{dr_s(t)}{dt} = \epsilon\, U_\infty \left(1 - \frac{r_s(t)}{r_o(t)}\right) \qquad (10)$$

If a current is impulsively applied at some initial time, and remains constant thereafter, Eq. (10) indicates that the shock position approaches the steady state shock position given by Eq. (9) exponentially with an e-folding time $\tau = r_o/\epsilon U_\infty$. This analysis, however, is based on the simplifying assumptions listed earlier in Section II, so that the steady state position given by Eq. (9), and the e-folding time are not quite correct. While a correct quasi-steady analysis taking the entire flow field into account would be very difficult, the accuracy of Eq. (10) is improved if we use the more precise definition of r_o for the steady state case from Eq. (6)(with the modification that I is taken as a function of time). For all of the later calculations, therefore, we have used Eq. (10) with r_o defined by Eq. (6).

In our experiments, the current was generated by the sinusoidal discharge of a capacitor bank. Thus, Eq. (6) becomes

$$r_o(t) = \frac{\sigma_s \epsilon^2}{\rho_\infty U_\infty} \left(\frac{\mu_o I_o \sin \omega t}{2\pi}\right)^2 \equiv r_{oo} \sin^2 \omega t \qquad (11)$$

Defining the characteristic time $\tau = r_{oo}/\epsilon U_\infty$, Eq. (10) becomes

$$\frac{d\, r_s(t)}{dt} + \frac{r_s(t)}{\tau \sin^2 \omega t} = \frac{r_{oo}}{\tau} \qquad (12)$$

This equation may be solved for r_s as a function of time for given values of ω, τ, r_{oo}, and initial conditions of r_s.

On the basis of the preceding considerations, calculations were made for air at 0.25 mm initial pressure, and a 50% argon - 50% oxygen mixture, at 1 mm initial pressure. Figure 2 shows plots of r_o vs U_s calculated from Eq. (6) for several values of current for these two test gases. The limits on shock velocity imposed by the Hall parameter and the upstream conductivity are indicated. For air, at $U_s = 8 \times 10^3$ m/sec and $p_i = 0.25$ mm, $\epsilon = 1/7$ and for $r_o = 2$ cm, (which requires a current of 2.7×10^5 amps), the characteristic flow time, τ, is 17.5 μsec. This is about equal to the average test time achievable in the shock tube used, and was found to be insufficient test time to perform easily interpretable experiments. The corresponding conditions for the argon-oxygen mixture at $p_i = 1$ mm, $U_s = 5 \times 10^3$ m/sec and $r_o = 5$ cm are: $\epsilon = 1/4$, $I = 4 \times 10^5$ amp, and $\tau = 40 \mu$sec with a test time of about 90 μsec.

A few runs were made in air. Their main value to this experiment is that photographs showing the two-dimensional character of the flow were taken. Also, since the density ratio, ϵ, for air is smaller than for the argon-oxygen mixture, thinner shock layers will be expected in air. The detailed results of one of these runs will be presented in the next section.

Our attention will be focused on the experiments performed in the argon-oxygen mixture because test times more than twice as long as the characteristic time for steady flow are available. For these experiments, the capacitor bank had a quarter cycle time of 90μsec, which resulted in an electric field due to dB/dt that has a maximum value less than a quarter of the maximum value of $\epsilon U_\infty B$. Since these maximums are 90° out of phase the effects of this spurious electric field can be ignored. Through the use of Eq. (12), the quasi-steady theoretical shock position (r_s) may be calculated as a function of time. The initial conditions are determined in the following way: When the incident shock arrives at the wire, $r_s = r_c$, the radius of the cylinder containing the straight wire. (The geometry of this cylinder will be discussed later.) Defining the time between the firing of the capacitor bank, and the arrival of the incident shock waves as Δ, Eq. (12) has the initial condition that $r_s = r_c$ at $t = \Delta t$. Figure 3 is a plot of the solution to this equation for Δt = 20, 40, 60, 80, 100, 120 μsec; $\tau = 40$ μsec; $\omega = 2 \times 10^4$ rad/μsec and $r_{oo} = 5$ cm, which is the steady state position resulting from Eq. (6) when $U_s = 5 \times 10^3$ m/sec, $p_i = 1$ mm, and $I = 4 \times 10^5$ amps.

Also shown in Fig. 3 is a plot of equivalent steady state shock position r_o [Eq. (11)] as a function of time for a sinusoidally varying current of the same frequency. From Eq. (10) we may note that the maximum shock position, $dr_s/dt = 0$, occurs at $r_s = r_o$. Thus at this maximum, the shock location is given by the steady state theory [Eq. (6)] evaluated at the instantaneous current which is flowing.

SECTION IV

EXPERIMENTAL EQUIPMENT

The experiments were performed in a shock tube with a driver in which helium is joule-heated by the rapid discharge of electrical energy. This device is thoroughly described in Ref. 18. Here, only a brief description will be given in order to demonstrate that the device is capable of producing a uniform test gas.

The tube consists of a driver section of 1.5-in. diameter of variable lenghts up to 1 ft. A diaphragm designed to burst at about 10,000 psi is located at the end of this driver section. The driver is coupled to the rest of the shock tube through a conical transition section, about 1 ft in length, in which the diameter changes linearly from the 1.5-in. to 6-in. The remaining part of the shock tube consists of 30 ft of 6-in. pipe, the first 20 ft being aluminum and the last 10 ft Pyrex glass. A conventional dump tank following the test section terminates the device.

Shock velocities and attenuation histories have been obtained over the entire length of the tube through the use of collimated photomultiplier and thin film heat transfer gauges mounted in the side wall. The values of shock velocities calculated from driver energy density considerations are in excess of the measured velocities by about 30%. This discrepancy has been attributed to energy transfer inefficiencies, ionization and radiation losses, and shock attenuation.[18]

Theoretical calculations have been made on the loss of ideal test time due to mass flow in the boundary layer, based on the work of Roshko[20] and Mirels.[21] Other effects, such as turbulent mixing, and Taylor instabilities, in fact, limit the test time to about half of this value. A number of diagnostic techniques have been used to experimentally determine the existence and duration of the test gas. These include mirror camera and image converter photographs, time resolved racetrack spectrograms, and photomultiplier traces. Figure 4 contains three instantaneous image converter photographs showing the shock front, test gas, and contact interface, as well as two photomultiplier traces of the same shock front displayed on a dual beam oscilloscope. These data were obtained in air at an initial pressure of .25 mm and a shock velocity of 8.8 mm/μsec. In both the image converter pictures and photomultiplier traces, the radiation overshoot characteristics of shock heated air is observed, as well as the region of relatively constant but less intense radiation following the luminous front. An irregular region of very intense radiation follows this equilibrium zone and is separated from it by the contact interface. The gases in this region are mostly driver gases and contaminants ablated from the driver wall.

This same type of photomultiplier data has been obtained in 50-50 mixtures of oxygen and argon at an initial pressure of 1 mm Hg, and several shock velocities, as indicated in Fig. 5. The photomultiplier oscillograms for the higher velocity case show a sharp rise when the shock arrives then a period of approximately 70 μ sec of uniform radiation from the test gas, and another sharp rise at the contact interface. At slightly higher velocities, a radiation overshoot at the shock, similar to the air situation, was observed. As the velocity was decreased, the radiation from the test gas in the visible part of the spectrum decreased very sharply. This is due to a different radiation mechanism at the lower velocities. At the high velocity, all of the oxygen is dissociated, and a few percent of the oxygen atoms have been ionized. As a result, the dominate radiation is Bremsstrahlung. At the lower velocities, however, there are still a significant number of oxygen molecules (5%) and there are almost no electrons (.001%). Hence, the Bremsstrahlung radiation is almost completely absent, and all that is observed is the molecular radiation from oxygen (Schumman-Runge). This lower level radiation is observed in the second oscillogram on Fig. 5, showing the results of a run at 4.7 mm/μsec. The oscillogram contains two traces at different sensitivities of a single photomultiplier. The upper trace, at the higher sensitivity, shows the arrival of the incident shock, followed by a continually increasing radiation level. The lower trace, at a sensitivity comparable to that for the higher velocity run, shows the luminosity increasing as the interface is approached, finally reaching a value comparable to the driver gas radiation level. The continual rise in radiation through the test gas is attributed to the small, but finite shock front velocity attenuation. Thus, the gas in the back of the test slug, which has a higher radiation level, was heated by a stronger shock than was the gas immediately behind the shock. Measurements of shock attenuation indicate that in the length of tube required to generate 100 μ sec of test gas, the incident shock has been attenuated by about 10%. Noting that the difference between shock velocities for the two runs shown in Fig. 4 (b) is on this order, it is not unreasonable to expect the test gas radiation at the lower velocity to change as indicated. Most of the experimental runs were made at velocities between these two limits.

In spite of the fact that the small change in initial shock velocity due to shock attenuation cause very large changes in the radiated light from the test gas, the values of density, temperature, conductivity, etc. behind a standing shock formed in this test gas are very insensitive to these small velocity changes.

As indicated earlier, the magnetic field within the shock tube was produced by discharge of a 10^3 μf bank of energy storage capacitors rated at 10 KV. A high pressure lovatron switch was connected on the hot side of the capacitor bank. In order to have the quarter-cycle time of the capacitor bank large compared with the e-folding time, as discussed earlier, it was necessary to have a highly inductive load. This was partially accomplished by inserting four straight wires across the shock tube rather than a single wire as originally used in the air experiments. The four wires were close to each other compared with the shock detachment distance, so that

the magnetic field at the shock position produced by currents flowing in the same direction in each wire were very close to the field produced by a single straight wire. The external connections were designed to provide additional inductance so that a quarter cycle time of about 90 μsec was achieved. This was a little more than twice the e-folding time of the flow geometry.

The general arrangement of this four wire assembly, installed in a model of the test section, is shown in Fig. 5. A 3/4-in. diameter epoxy clad fiberglass rod was used as a core for that part of the four wire assembly placed inside the shock tube. The choice of this material was determined by the extremely large compressive stresses placed on the core. Unclad plastics, such as teflon, nylon, and even nylon phenolic, quickly disintegrated under the load. Four slots equally spaced around the rod, and parallel with the rod axis, were provided to position the conductors. In order to provide insulation between conductors in the low pressure environment of the shock tube, a 1/8-in. thick layer of fiberglass saturated with epoxy resin was wound around the assembly. This brought the finished diameter of the cylinder to one inch.

Measurements of shock velocity, as well as oscilloscope and capacitor bank triggering were accomplished through the use of a series of 4 thin film heat transfer gauges located 50 cm apart upstream of the wire assembly. The choice of heat transfer gauges rather than photomultiplication was based on the extreme sensitivity of test gas radiation intensity to initial shock velocity, as discussed earlier. The output of the gauge located furthest upstream of the experiment was used to trigger the oscilloscopes, the capacitor bank (through a delay) and some photographic equipment. Arrangement of experimental equipment is indicated in Fig. 5(a). The output of the three guages downstream was monitored on dual beam oscilloscopes in order to measure shock velocity. Also displayed on an oscilloscope was the output of a Rogowski coil used to measure the current flowing through the wire in the experiment.

For the majority of the runs, the mirror camera was the only quantitative diagnostic measurement of flow geometry. For these runs, the 4-wire cylinder assembly was inserted across the diameter of the test section parallel with the test section windows. The mirror camera was aligned with its axis perpendicular to both the flow direction and the cylinder. A viewing slit 1 mm wide was placed in the center of the test section window, and restricted the field of view of the mirror camera to a region 5-1/2 cm upstream and 2 cm downstream of the center of the cylinder. The hexagonal mirror of the camera was spun at about 6×10^4 rpm, giving writing speeds of the order of .04 mm/μsec on the film.

For most runs, a spark plug, located in the field of view of the mirror camera, was fired at the time the capacitor bank fired. In this way, an independent check on the timing could be obtained.

The last few runs were made with the cylinder inserted through the test section windows, as shown in Fig. 5(b). For these runs, an STL image converter camera, which was capable of taking these photographs at 8 μsec intervals with 0.1 μsec exposure times, was aligned along the axis of the cylinder. Its field of view was a square 10 cm on a side-centered around the cylinder. A circle 8 cm in diameter and a line parallel to the stagnation streamline were marked on the viewing window for reference. The mirror camera was located on the opposite side of the test section and viewed the flow through a slit parallel to the stagnation streamline and extending upstream 5 cm, aligned in the same manner.

SECTION V

EXPERIMENTAL RESULTS

A total of approximately 20 successful runs was made in the 50-50 mixture of argon and oxygen. For all of these runs, the initial shock tube pressure was 1 mm Hg, and the range of shock velocities was between 4.3 and 6 mm/μsec. Most of the runs were made at effective straight wire currents of 4×10^5 amp, resulting in a magnetic field of about 2 webers/m^2 at the steady state shock position, and magnetic Reynolds numbers less than 0.1. Some typical photographic results at currents of 4×10^5 amps are shown in Figs. 6, 7, 8 and 9. For the runs shown in Figs. 6 and 7, only the mirror camera with its axis perpendicular to the flow and the cylinder was used. Both mirror camera and image converter results are shown in the latter two figures, for which the cameras were aligned along the cylinder axis. To facilitate the understanding of the mirror camera photographs in all the figures, x-t diagrams have been constructed to the left of the photographs on the basis of the velocity data obtained from the heat transfer gauges. For some of the runs, the mirror camera slit was not aligned exactly parallel to the flow direction, with the result that the light streaks at the interface on the photograph are not parallel with the interface marked on the x-t diagram. For the runs in which a spark plug was used to mark the mirror camera at the time the bank fired, such as Fig. 6, an independent check on the oscillogram timing data could be made. These checks indicated that the shock arrival time could be predicted within approximately 5μsec.

When operating in the 50-50 argon-oxygen gas mixtures at velocities below 5.1 mm/μsec the difference in light intensity between the free stream (Schumann-Runge radiation) and the gas behind the standing shock (Bremsstrahlung radiation) was so great that in order to prevent the radiation from the standing shock from overexposing the film, the camera had to be closed down to the point where the radiation from free stream gas did not expose the film. However, this presented no problem since a visible standing shock appeared as soon as the incident shock arrived at the cylinder. From the mirror camera photographs, it is seen that a standing shock moves out from the cylinder, in general accordance with the theoretical prediction (solid white line) taken from Fig. 3 for the particular Δt of each experimental situation and modified by the results of Fig. 2 for the particular velocity of the run.

Toward the end of the test time, it will be noticed that the radiation from the standing shock appears to grow dimmer. This can be explained as follows. The predominant radiation from the standing shock, as indicated, is Bremmstrahlung, which varies as the square of the electron number density. Calculations of the electron number density behind a standing normal shock, and a shock reflected from an end wall, indicate that while the temperature does not change very much, the electron number density is lower behind the

standing shock by a factor of 2 or 3. Since, in our experiments, the standing shock intially moves upstream at about the same velocity as a shock reflected from an end wall, its radiation will be greater by a factor of 2^2 or 3^2 while it is moving than when it stands stationary. Under the same conditions, shock layer conductivity depends only on collisions between electrons and oxygen ions. The Coulomb cross section for this type of collision can be expressed analytically,[19] resulting in an equation for conductivity that depends only on the temperature to the three halves power, and virtually independent of electron number density. Hence, even though there is a variation in electron number density large enough to produce significant changes in radiated light, these variations cause little change in the conductivity since the change in temperature is small. This phenomenon of more radiation from a standing shock that has not reached its equilibrium position has also been observed in the pure aerodynamic case with no magnetic field.

One other unusual phenomenon deserves mention. It is observed from Figs. 6 and 7, for which the mirror camera was aligned perpendicular to the cylinder, that about 75 μsec after the bank fires, a wave, which starts from behind the cylinder, moves upstream at about 0.5 mm/μsec. This wave is probably due to the fact that the flow above and below the stagnation streamline particularly near the cylinder ends, passes through a complicated shock system which reduces the flow Mach number to a value sufficiently small to cause choking. Since the sonic line is located at an angle of about 45° to the flow direction, the choking wave does not interfere with conditions at the stagnation point until it has moved out approximately 0.7 r_o. No such secondary wave is observed in the mirror camera photos taken with the camera aligned along the axis of the cylinder, as in Figs. 8 and 9. This is consistent with the previous arguments because the field of view of the camera is restricted to the region very close to the axis of the flow, or the incoming stagnation streamline, and this camera is therefore unable to see anything happening above or below the cylinder.

The image converter picture of these runs, and the times at which they were taken, are also shown in Figs. 8 and 9. The f number of both cameras was increased by a factor of 10 from Fig. 8 to Fig. 9. Thus, the image converter photographs of Fig. 8 show a great deal more detail of the flow, including some indication of a wake behind the cylinder, than shown in Fig. 9. These image converter photographs also give a good indication of the manner in which the shock follows the circular field line. This may be seen by comparing the wave front with the 4 cm radius circular grid through which the photographs were taken. In Fig. 9 a gradient in light intensity, indicating a density gradient, is visible along the stagnation streamline.

As previously indicated, some early runs were made using air as a test gas. This had the advantage of smaller density ratios ($\epsilon = 1/7$), resulting in a thinner shock layer (ϵr_0). The test time at the shock velocity required to satisfy the limitation on the Hall parameter and free-stream conductivity, was rather small (15-20 μsec) compared with e-folding times for a 2 cm shock detachment distance of $\tau = 17.5$ μsec. For these runs, the four wire assembly shown in Fig. 4 was replaced by a single 3/16-inch diameter copper wire. With

the shock tube operating at shock velocities of about 8 mm/μsec at an initial pressure of 0.25 mm capacitor bank quarter cycle time of 40 μsec, and a current of 2.8×10^5 amps, the theoretical steady state shock position was 2 cm. Figure 10 shows the result of one interesting run in air. For this run the mirror camera was aligned along the axis of the 3/16-inch wire, and the image converter had its axis perpendicular to both the wire and the flow direction. Its field of view covered the center 7 cm of the rod, as well as a few cm upstream and downstream. The timing and velocity measurements for this run were obtained from three photomultipliers located at various positions upstream of the wire.

As in the three previous figures, an x-t diagram could be constructed to the left of the actual mirror camera photograph. When the bank fires, a disturbance of some sort occurs and appears to propagate upstream until it intersects the incident shock. At this point, it is swept back downstream at the flow velocity. The main body of the test gas remains unaffected by this disturbance, since most of the test gas passed through the shock before the point where the disturbance intersects the shock. As the disturbance approaches the rod, it slows down and appears to give way to a standing MHD-supported shock wave. This process is quite a contrast from the manner in which the standing shock is formed in the previously described runs made in the argon-oxygen mixture. The disturbance is probably an electrodeless discharge created by the electric field parallel with the wire which, because of the relatively high quarter cycle time for these runs had a maximum value almost equal to $\epsilon U_\infty B$. The discharge ionized the gas, which then moved upstream on the expanding magnetic field lines.

Also shown in Fig. 10 are the image converter picture and the times at which they were taken. These image converter photographs, as well as similar photographs taken during the other runs, indicate that the shock layer is uniform along the 15 cm rod to within about 1 or 2 cm of the shock tube wall, thus validating a two-dimensional analysis.

One other aspect of the two-dimensional nature of the flow deserves mention. The currents in the gas which flow in the shock layer are supposed to close on themselves. Since no external path has been provided for this to happen, the currents must close somewhere in the region of hot gas surrounding, or downstream of the cylinder. In order to determine how well the gas currents are able to close, successful measurements in the argon-oxygen case were made of the electric field in the shock layer. Except for a small pulse when the shock arrived, the value of the electric field within the shock layer was very much less than $\epsilon U_\infty B$. This indicates that the electric field was driving a current through the gas determined by $\sigma_s \epsilon U_\infty B$ and that the resistance of the rest of the circuit through which the current closed was small. The value of the small pulse of electric field measured when the incident shock arrived corresponds to $\epsilon U_\infty B$, and indicates that initially no path is provided for the currents to flow. The time required for this pulse to disappear is the time required to set up a return path for the gas currents, and corresponds approximately to the time it takes the incident shock to move a few centimeters.

SECTION VI

COMPARISON WITH THEORY

Before making any quantitative comparisons between the theory and experiments, an estimate of the validity of the theoretical calculations will be presented. It will be recalled from Section II that the Levy-Petschek expression for the shock stand-off distance, Eq. (6), is only valid when $\sqrt{2\epsilon}$ is much less than unity. In the experiments conducted in the argon-oxygen mixture, however, this quantity is only 0.7, which is hardly small. In addition, the Levy-Petschek theory should not be expected to be any more accurate in describing the MHD-supported shock stand-off distance than similar analyses, such as one presented by Hayes and Probstein,[22] are at describing the corresponding aerodynamic situation. In this latter case, even at small values of ϵ, the theory including only first order terms in ϵ gives values of shock detachment distances only 60% as large as the experimental data reported in Liepmann and Roshko,[23] which agree well with our own zero magnetic field data. There are, of course, numerical calculations for the aerodynamic case, such as that of Belotserkovskii,[24] which involve stepwise integration of the flow equation from the shock to the body. In view of the above considerations, there is no reason to expect the theoretical predictions given in Figs. 2 and 3 to agree with the experiments by any more than a factor of two.

Figure 11 shows a plot of the shock position data obtained in the argon-oxygen mixture, as a function of current. Runs were made at various shock velocities between 4.3/μ sec and 6 mm/μ sec. While most of the runs were made at various effective single wire currents of 4.0×10^5 amps, a number of runs were made at 3.3×10^5 amps.

The data points for this figure are obtained directly from the mirror camera photographs in the following manner: For every run, the shock position was measured from the mirror camera film at the time when the theoretical shock position was at its maximum value, according to Fig. 2. This stand-off distance was plotted against the instantaneous current flowing at that time. This particular point was chosen to represent the entire run because at this time, $dr_s/dt = 0$, and momentarily the shock position is at a steady state. A number of curves for the range of shock velocities covered by the experiment, as well as the location of the leading edge of the cylinder, and an aerodynamically supported shock are also shown. Regarding the latter, the experimental data reported by Liepmann and Roshko,[23] were used.

In Fig. 12, all of the data have been normalized to a shock velocity of 5mm/μsec according to the theoretical variation of shock position with velocity given in Fig. 2. In this figure, we see that the data for shock velocities below 5.1 mm/μ sec scatter less than 10% around a mean, which is

almost coincident with the theoretical calculation. This good agreement with theory must be interpreted in light of the expected accuracy of the theory discussed earlier.

At velocities above 4.2 mm/μsec, the shock had moved upstream of the limited field of view of the mirror camera well before maximum current was reached. These points were normalized to maximum current by multiplying the measured shock position by the ratio of the maximum theoretical shock position (Fig. 2) to the theoretical shock position at the time in question. These data begin to depart significantly from theory. This result, although expected at a slightly higher velocity, is in general agreement with the fact that the free stream becomes significantly conducting at high shock velocities, as indicated in Fig. 2, thus changing the nature and extent of the interaction.

From the data presented, it is difficult to determine the effect of a large Hall parameter on the shock location because at the low velocities required for this to occur (4.5 mm/μsec) the theoretical shock position is close to the aerodynamic shock position.

SECTION VII

CONCLUSIONS

The results of a shock tube experiment in which the magnetic field from a straight wire perpendicular to the flow interacted strongly with a hypersonic streaming flow are in good agreement with a theory proposed by Levy and Petschek. Although their theory was for a steady state, calculation of the variation of shock detachment distance with time, based on a quasi-steady model applied to the time variations of the magnetic field used in the experiments, agreed well with the mirror camera data. At intermediate shock velocities, comparison of the experimentally measured shock position (at a time corresponding to the time at which the quasi-steady theory predicts a maximum detachment distance) differ by less than 10% from the steady state theoretical prediction (based on the instantaneous current flowing at that time). This agreement is surprisingly good in view of the fact that terms of the order of $\sqrt{2\epsilon}$ were ignored in the theory, and the experiments were performed at a value of $\epsilon = 1/4$. At high velocities, corresponding to large free stream conductivities, the experimentally measured shock position was considerably larger than that predicted by theory. No strong conclusions could be drawn concerning the shock position at low velocities where the Hall parameter becomes significant. Both image converter and mirror camera photographs indicated that the density behind the shock wave dropped quickly through the shock layer. This was particularly apparent for the experiments performed in air, due to a smaller density ratio, and therefore a smaller shock layer thickness. Image converter pictures showing the curvature of the shock indicate that it follows field lines quite closely up to about 45° from the stagnation streamline.

REFERENCES

1. Levy, R. H. and Petschek, H. E., "Magnetohydrodynamically Supported Hypersonic Shock Layer," Phys. Fluids 6, 7, 946-961, July 1963.

2. Patrick, R. M. and Brogan, T. R., "One-Dimensional Flow of an Ionized Gas Through a Magnetic Field," J. Fluid Mechanics 5 289, February 1959.

3. Kantrowitz, A. R., "Flight Magnetohydrodynamics," published in Symposium of Plasma Dynamics, ed. by F. H. Clauser, Reading, Mass.: Addison Wesley, 1960, pp. 221-232.

4. Fishman, F., Lothrop, J. W., Patrick, R. M., Petschek, H. E., "Supersonic Two-Dimensional Magnetohydrodynamic Flow," published in The Magnetohydrodynamics of Conducting Fluids, ed. by D. Bershader. Standford University Press, 1959, pp. 90-119.

5. Kemp, N. H. and Petschek, H. E., "Two-Dimensional Incompressible Magnetohydrodynamic Flow Across An Elliptical Solenoid," J. Fluid Mech. 4, 553, November 1958.

6. Bush, W. B. and Ziemer, R. W., "Magnetic Field Effects on Bow Shock Stand-Off Distance," Phys. Rev. Letters, 1, 58, July 1958.

7. Bush, W. B., "Magnetohydrodynamic-Hypersonic Flow Past a Blunt Nose," J. Aero-Space Sciences, 25, 11, 685-690, November 1958. See also Bush, W. B., "A Note on Magnetohydrodynamic-Hypersonic Flow Past a Blunt Body," J. Aero-Space Sciences, 26, 8, 536, August 1959.

8. Kemp, N. H., "On Hypersonic Stagnation Point Flow with a Magnetic Field," J. Aeronautical Sciences, Readers' Forum, 25, 6, 405-407, June 1958. See also Freeman, N. C., "On the Flow Past a Sphere at Hypersonic Speed with a Magnetic Field," J. Aero-Space Sciences, 26 10, 670-672, October 1959 and Kemp, N. H. "Author's Reply," J. Aero/Space Sciences, 26, 10, 672, October 1959.

9. Neuringer, J. L., and McIlroy, "Incompressible Two-Dimensional Stagnation Point Flow of an Electrically Conducting Viscous Fluid in the Presence of a Magnetic Field," J. Aero. Sci. 25, 3, 194-198, March 1958.

10. Lykoudis, P. S., "The Newtonian Approximation in Magnetic Hypersonic Stagnation Point Flow," J. Aero/Space Sciences, 28, 7, 541-546, July 1961.

11. Josephson, V. and Hales, R. W., "Parametric Study of the Conical Shock Tube," Phys. Fluids 4, 373 (1961).

12. Cloupeau, M., "Interpretation of Luminous Phenomena Observed in Electromagnetic Shock Tubes," Phys. Fluids, 6, 5, 679-688, May 1963.

13. Keck, J., "Current Speed in a Magnetic Annular Shock Tube," Journal of Quantitative Spectroscopy and Radiative Transfer, 3,4, October - December 1963.

14. Pugh, E. R., "Studies of Phenomenon Occurring in an Electromagnetic Shock Tube," Doctoral Thesis, Cornell University Graduate School of Aeronautical Engineering, Ithaca, New York (1962).

15. Ericson, W. B., Maciulaitis, A., Spagnolo, R. A., Loeffler, A. L., Scheuing, R. A., Hopkins, H. B., "An Investigation of Magnetohydrodynamic Principles Applicable to Flight Control," Grumman Aircraft Engineering Corp., Bethpage, New York, December 1962.

16. Bostick, W. H., Byfield, H. Nakagawa, T., and Wilk, D., "Interaction Between Plasma and a Two-Dimensional Magnetic Dipole," Physics of Fluids, 5, 10, 1305-1307, October 1962.

17. Hurley, J., "Interaction of a Streaming Plasma with a Magnetic Field of a Line Current," Phys. Fluids 4, 1, 109, January 1961.

18. Camm, J. L. and Rose, P. H., "Electric Shock Tube for High Velocity Simulation," Phys. Fluids 6 5, 663-678, May 1963.

19. Lamb, Lawrence and Lin, S. C., "Electrical Conductivity of Thermally Ionized Air Produced in a Shock Tube," J. Fluid Physics 28, 754-759, July 1959.

20. Roshko, A., "On Flow Duration in Low Pressure Shock Tubes," Phys. Fluids 4, 1451, (1961).

21. Mirels, H., "Test Times in Low Pressure Shock Tubes," Phys. Fluids 6, 9, 1201 September 1963.

22. Hayes, W. D. and Probstein, R. F., Hypersonic Flow Theory Academic Press, New York, (1959).

23. Lipmann, H. W. and Roshko, A., Elements of Gasdynamics, John Wiley and Son, New York, (1956).

24. Belotserkovskii, O. M., "Flow Past a Circular Cylinder With a Detached Shock," Vychislitel naia Matematika 3 149-185, (1958), translated in Avco-Research and Advanced Development Division TM: RAD-9-TM-59-66, September 1959.

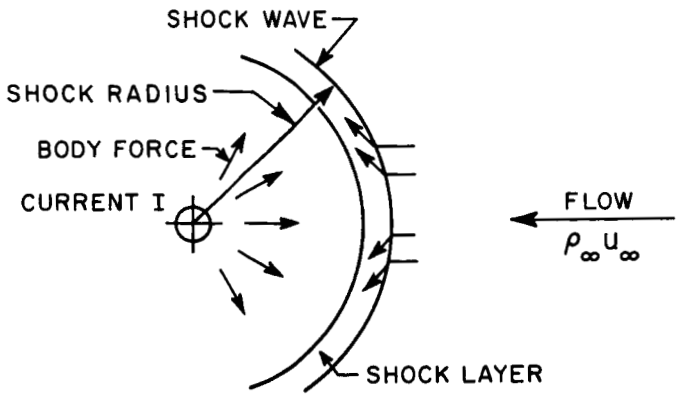

Fig. 1 Schematic drawing of the magnetohydrodynamically-supported hypersonic shock layer ahead of a current-carrying wire. The flow is conducting only in the shock layer.

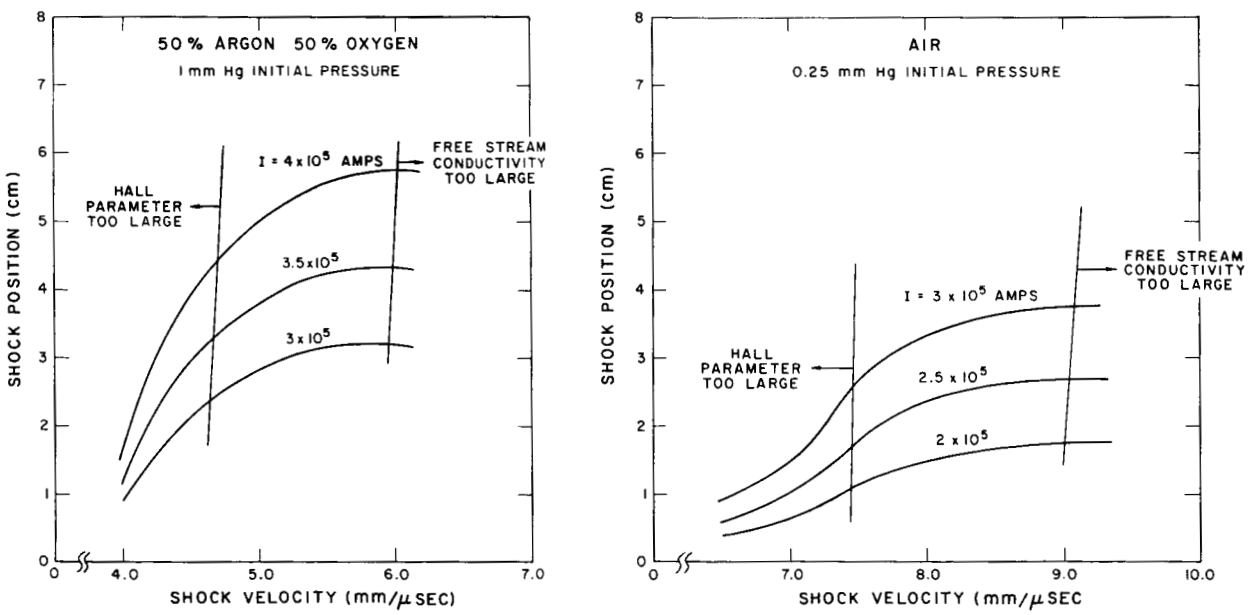

Fig. 2 Steady state theoretical predictions of MHD-supported shock detachment distance calculated for air and a 50-50 mixture of Oxygen and Argon in the shock tube.

8506

A2529

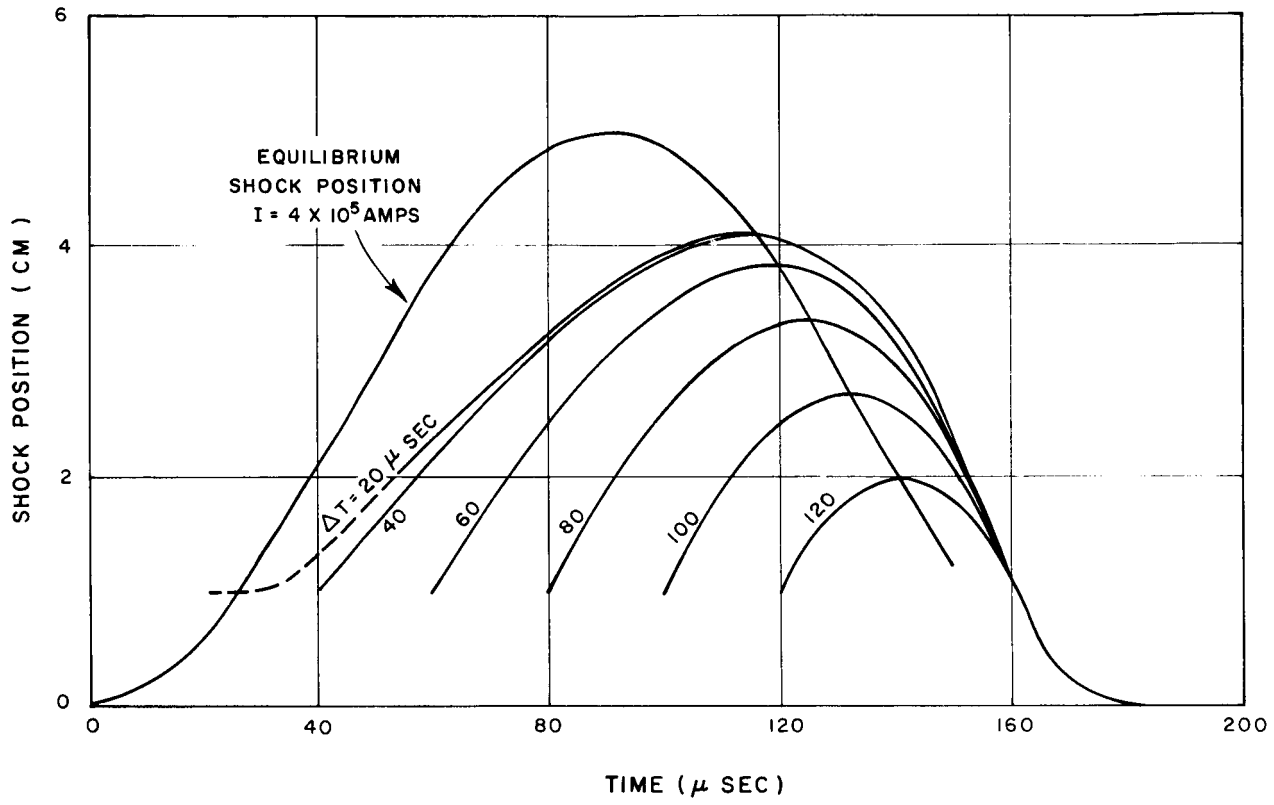

Fig. 3 Quasi-steady response of MHD-supported shock to a sinusoidally varying magnetic field, Eq. (12). Dotted portion of curve represents region in which aerodynamic forces, which are not included in the calculations, are larger then MHD forces.

A2531

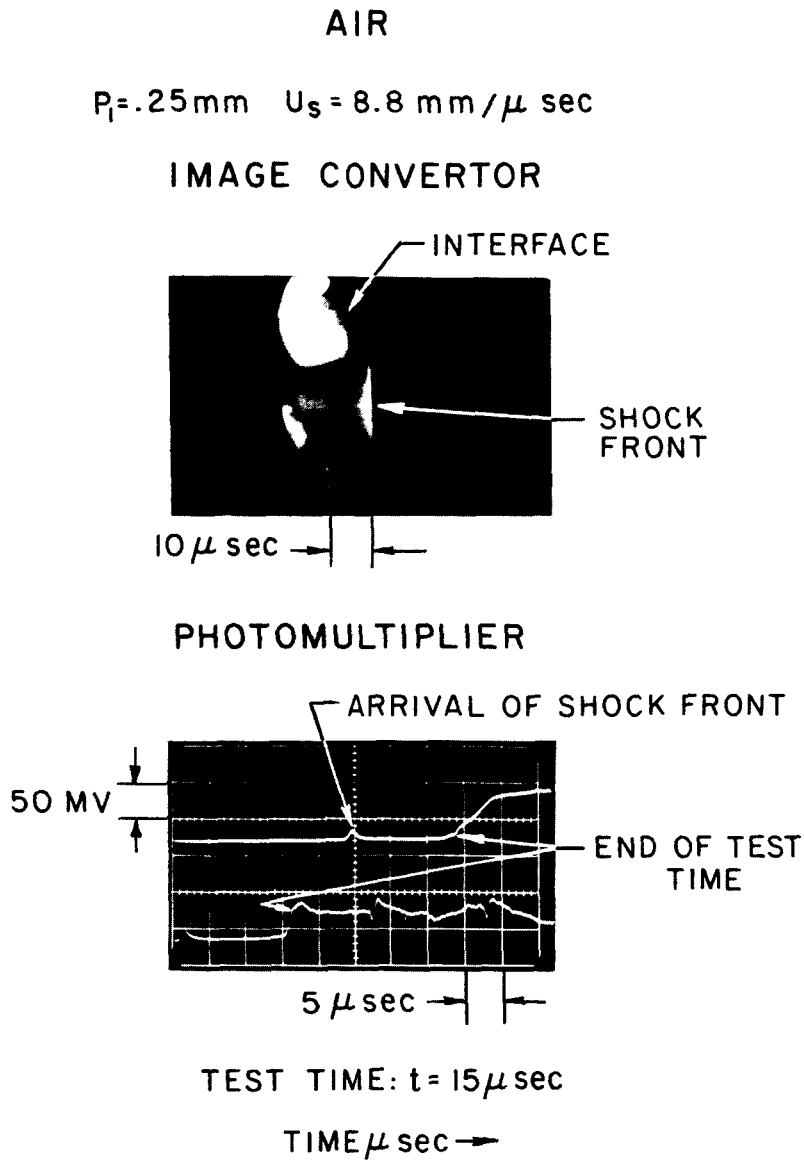

Fig. 4 Instantaneous photographs and photomultiplier oscillograms of the radiation in the visible range of the spectrum from shock-heated air and driver gas. There are three .05 μ sec exposures in the photograph, taken at 10 μ sec intervals by an image converter (STL Model C).

A2530

50% ARGON - 50% OXYGEN

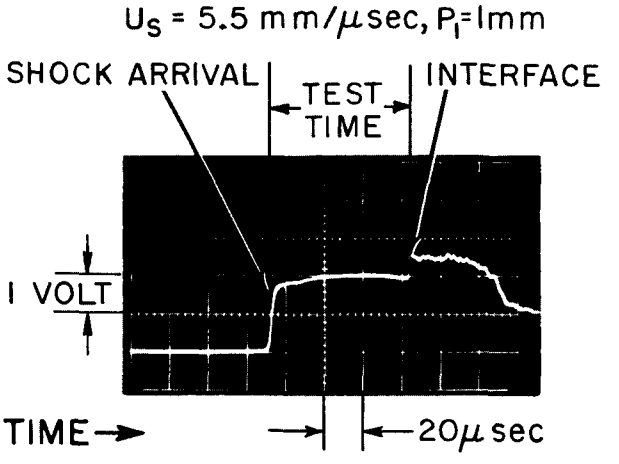

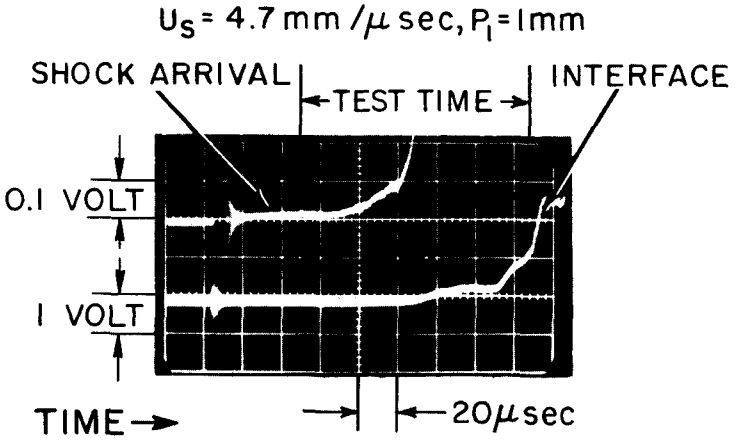

Fig. 5 Photomultiplier oscillograms of radiation in the visible range of the spectrum from shock-heated mixtures of 50% argon and 50% oxygen. Radiation from test gas for low velocity runs is Schumann Runge radiation from molecular oxygen, while at higher velocity Bremsstrahlung radiation dominates due to the higher electron concentration.

A2532

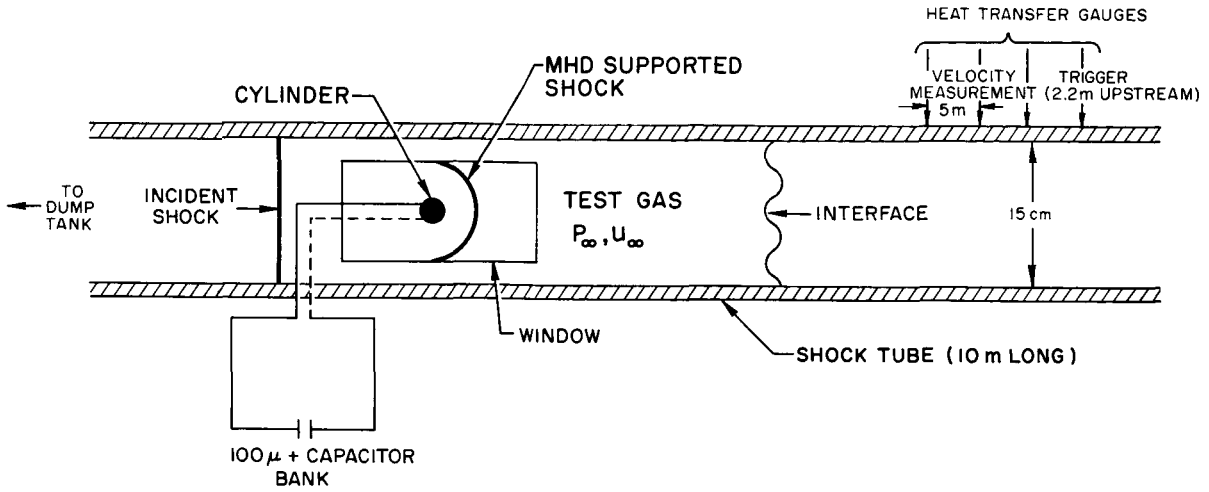

Fig. 6 Schematic diagram of experimental equipment used to study MHD-supported shock layer. Photographs of the flow luminosity were taken with a mirror camera and an image convertor, viewing both parallel with the cylinder, and perpendicular to both the cylinder and the flow direction.

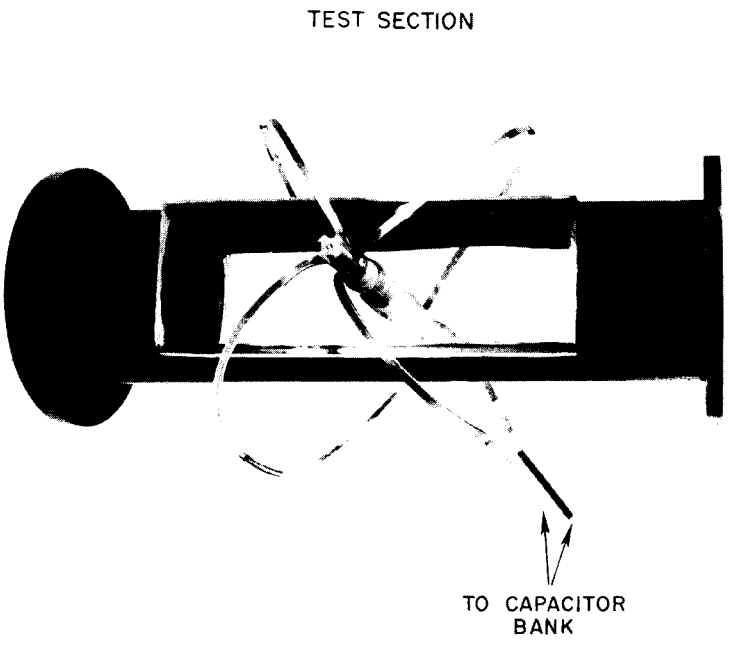

Fig. 7 Photograph of a model of the test section as installed in the shock tube. Photo shows the manner in which the four wires are inserted close to each other across a diameter of the shock tube.

A2533

A2534

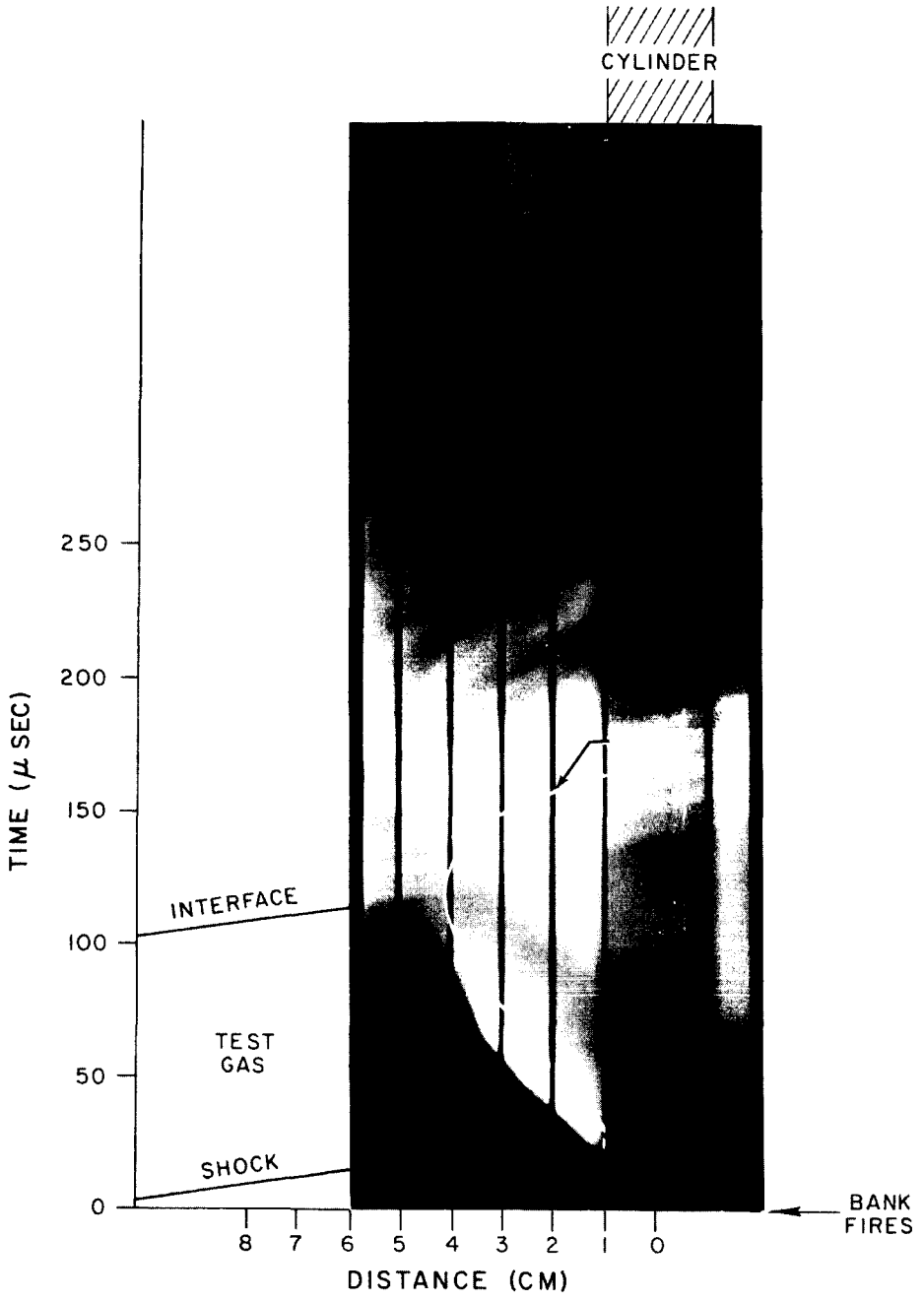

Fig. 8 Mirror camera photograph of run in 50% oxygen, 50% argon test gas at 1 mm Hg initial pressure and 5.0 mm/ μ sec shock speed. Mirror camera aligned perpendicular to cylinder and flow direction. White theory line drawn from Eq. (12). Dotted portion of line represents the region in which aerodynamic forces, which are not included in the calculation, are larger than MHD forces.

A2535

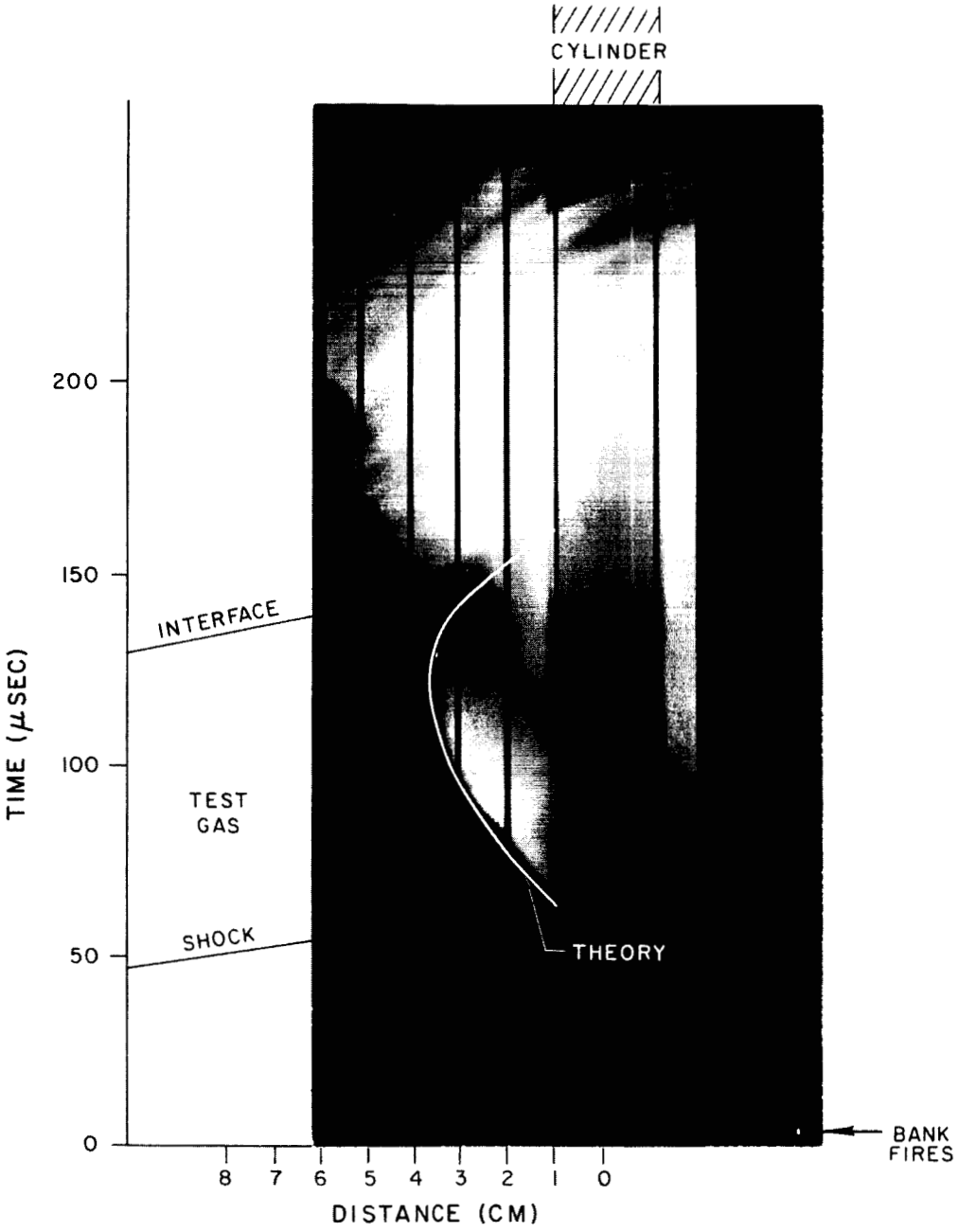

Fig. 9 Mirror camera photograph of run in 50% oxygen, 50% argon test gas at 1 mm Hg initial pressure and 4.9 mm/ μsec shock velocity. Mirror camera aligned perpendicular to cylinder and flow direction.

A2536

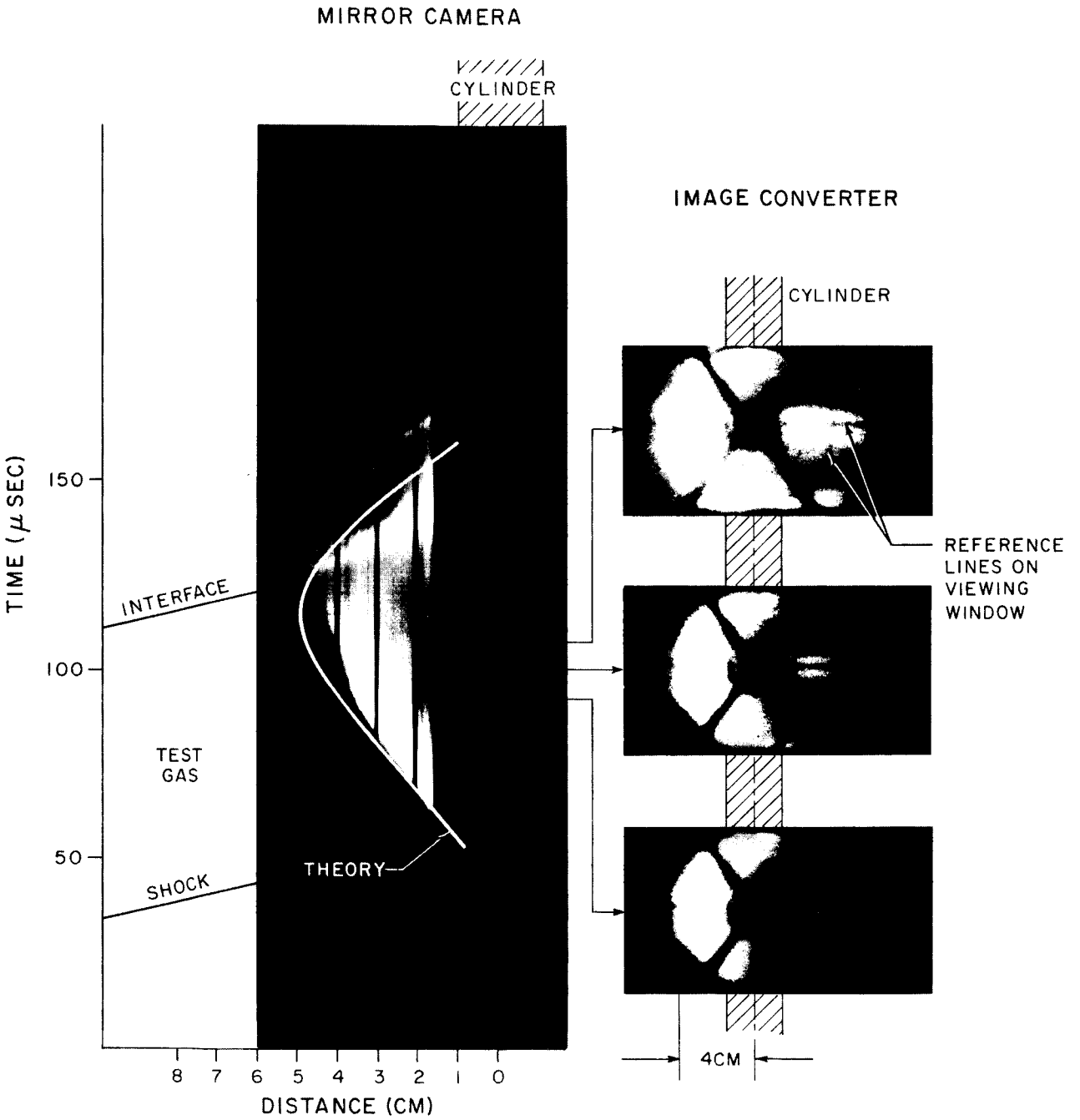

Fig. 10 Mirror camera and image converter (STL Model C) photograph of run in 50% oxygen, 50% argon test gas at 1 mm Hg initial pressure, and 5.0 mm/μsec shock velocity. Both cameras aligned along the axis of the cylinder.

A2537

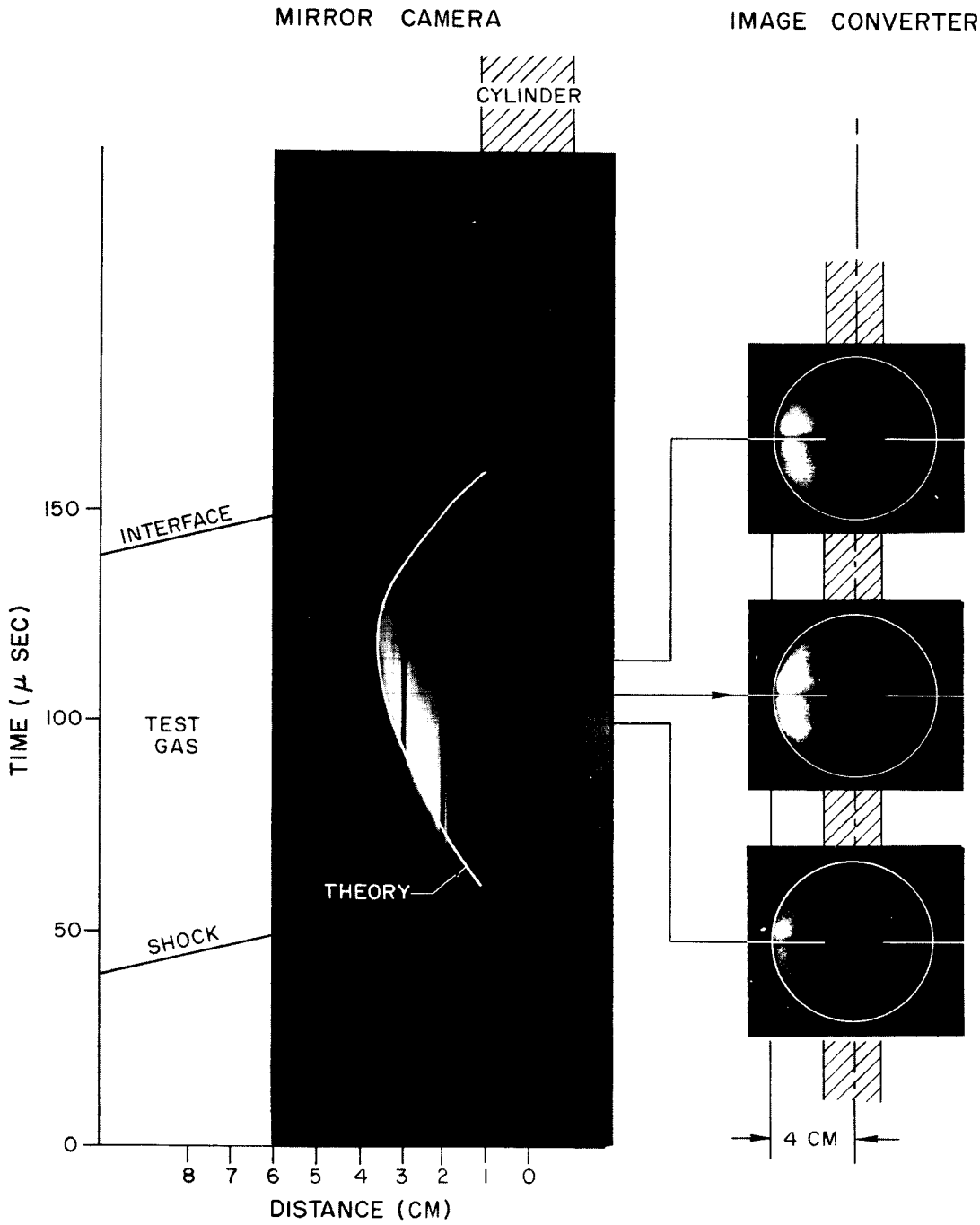

Fig. 11 Mirror camera and image converter (STL Model C) photograph of run in 50% oxygen, 50% argon test gas at 1 mm Hg initial pressure and 4.8 mm/μsec shock velocity. Both cameras aligned along the axis of the cylinder.

A2538

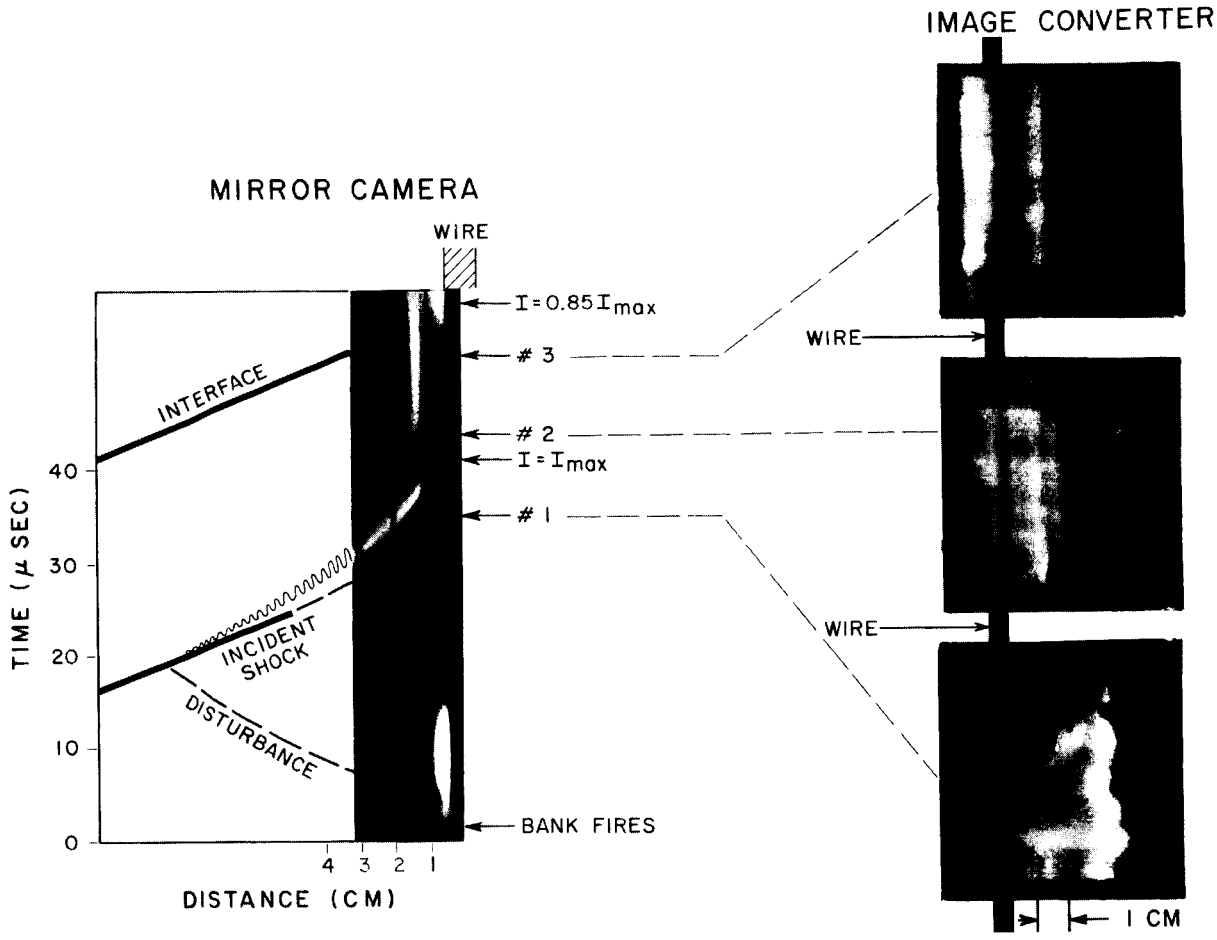

Fig. 12 Mirror camera and image converter (STL Model C) photographs of run in air at 0.25 mm Hg initial pressure and 8.0 mm/μsec shock velocity. Mirror camera aligned along axis of wire and image converter perpendicular to both wire and flow direction.

9418

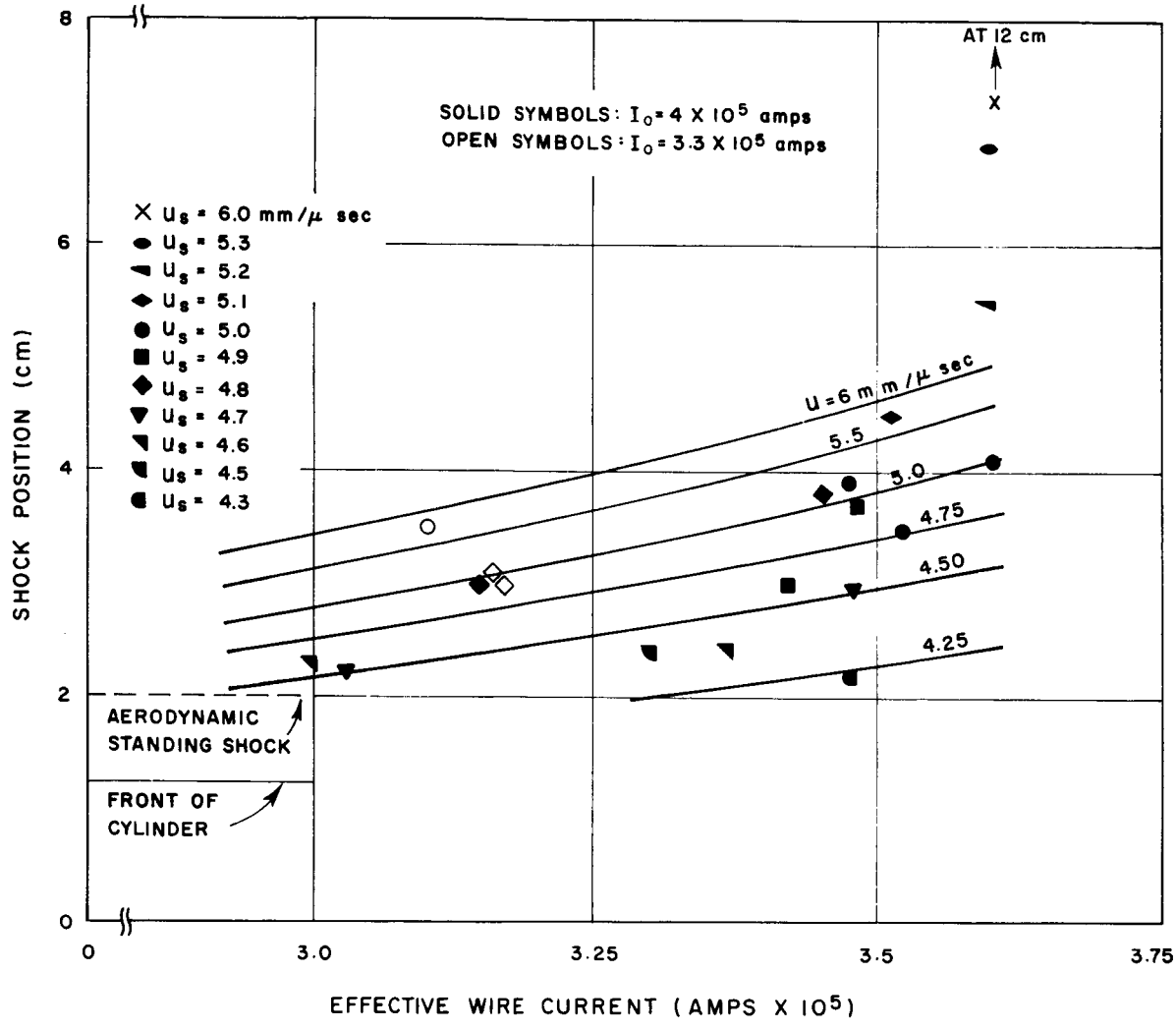

Fig. 13 Comparison of experimentally measured shock position with theoretical predictions. Data are plotted directly as read from mirror camera photographs, without any scaling.

A2539

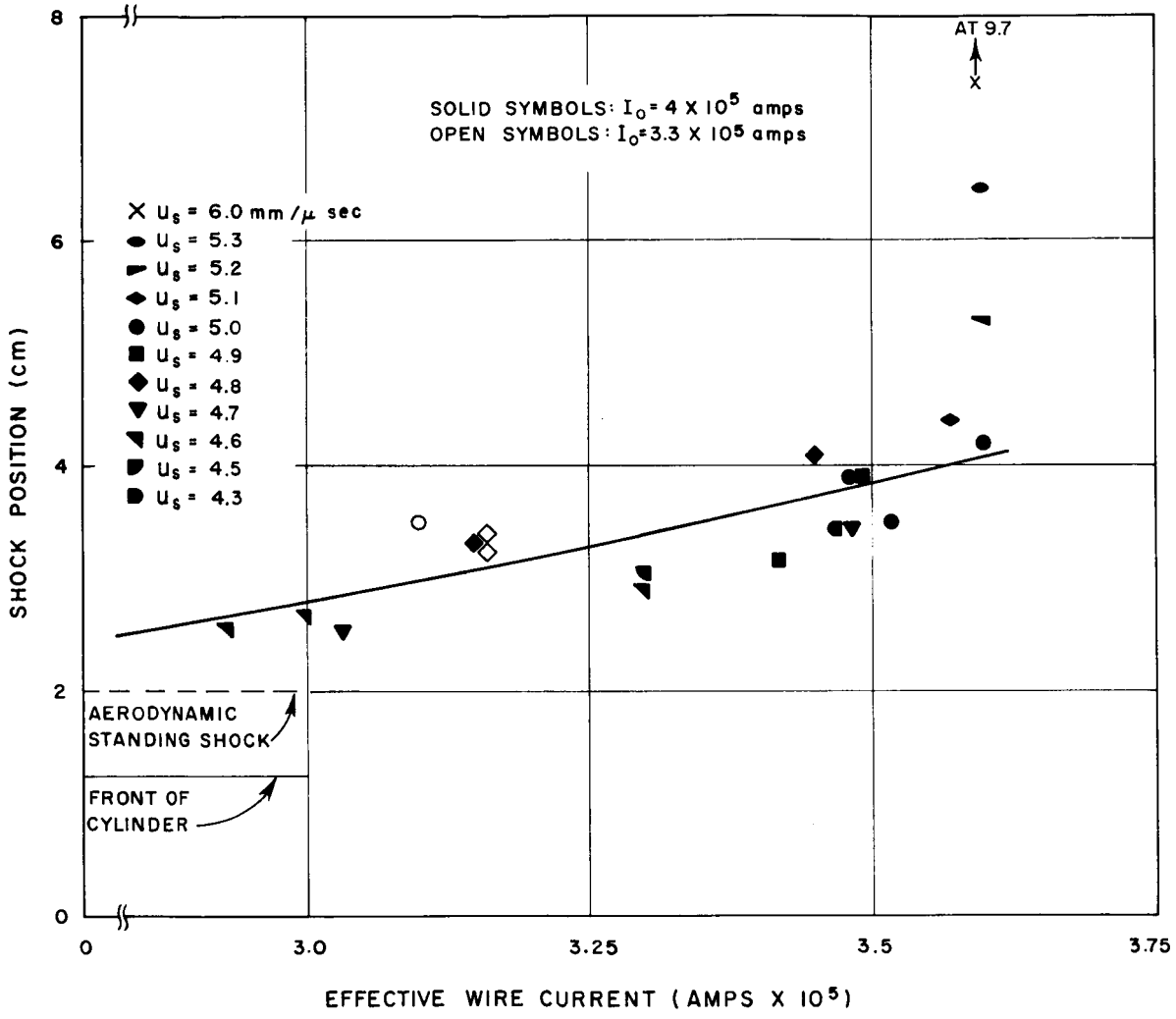

Fig. 14 Comparison of normalized experimental data on shock position with theoretical predictions. All mirror camera data are normalized to a shock velocity of 5 mm/μ sec.

A2540